# Nonhydrostatic simulations of tide-induced mixing in the Halmahera Sea: A possible role in the transformation of the Indonesian Throughflow waters

Taira Nagai, Toshiyuki Hibiya, Pascale Bouruet-Aubertot

AGU PUBLICATIONS

JGR

Journal of Geophysical Research: Oceans

RESEARCH ARTICLE

10.1002/2017JC013381

**Key Points:**
- The physical mechanisms for the transformation of the Indonesian Throughflow (ITF) waters in the Halmahera Sea are numerically investigated
- Nonhydrostatic experiments show that vertical mixing caused by breaking of internal tides dominates the transformation of the ITF waters
- Horizontal mixing associated with the tide-induced submesoscale eddies also plays a nonnegligible role in transforming the ITF waters

**Correspondence to:**
T. Nagai,
nagai_t@eps.s.u-tokyo.ac.jp

**Citation:**
Nagai, T., Hibiya, T., & Bouruet-Aubertot, P. (2017). Nonhydrostatic simulations of tide-induced mixing in the Halmahera Sea: A possible role in the transformation of the Indonesian Throughflow waters. *Journal of Geophysical Research: Oceans*, *122*, 8933–8943. https://doi.org/10.1002/2017JC013381

Received 23 AUG 2017
Accepted 4 OCT 2017
Accepted article online 10 OCT 2017
Published online 21 NOV 2017



# Nonhydrostatic Simulations of Tide-Induced Mixing in the Halmahera Sea: A Possible Role in the Transformation of the Indonesian Throughflow Waters

**Taira Nagai[1], Toshiyuki Hibiya[1], and Pascale Bouruet-Aubertot[2]**

[1]Department of Earth and Planetary Science, Graduate School of Science, The University of Tokyo, Tokyo, Japan, [2]Laboratoire d'Océanographie et du Climat: Expérimentations et Approches Numériques, Institut Pierre Simon Laplace (LOCEAN-IPSL), Sorbonnes Universités, UPMC Univ. Paris 06, Paris, France

**Abstract** The Indonesian Throughflow (ITF) waters are significantly transformed within the Indonesian Archipelago and consequently influence the large-scale ocean circulation such as Agulhas and Leeuwin Currents. Existing ocean general circulation models (OGCMs) are, however, incapable of reproducing the transformation of the ITF waters, since tidal forcing is neglected in such models. In the present study, we first conduct high-resolution nonhydrostatic three-dimensional numerical experiments focusing on the transformation of the ITF waters in the Halmahera Sea which is thought to be the most important bottleneck in simulating the ITF water mass properties. It is shown that intensive vertical mixing induced by breaking of internal tides in the shallow regions in the Halmahera Sea dilutes the ITF waters, significantly reducing model biases found in the existing OGCMs. We next evaluate quantitatively the effect of tide-induced vertical mixing on the transformation of the ITF waters. It is shown that tide-induced vertical mixing dominates the transformation of the ITF waters, although some supplementary processes such as horizontal mixing associated with the submesoscale eddies resulting from tidal interaction with land configurations cannot be ignored.

## 1. Introduction

The Indonesian Throughflow (ITF), which brings the relatively warm and saline Pacific waters into the Indian Ocean, plays an important role in the basinwide heat and freshwater budgets. The ITF water mass properties are significantly transformed while passing through the Indonesian Archipelago and consequently influence the large-scale ocean circulation such as Agulhas and Leeuwin Currents (Gordon, 2005; Tomczak & Godfrey, 2003).

The transformation of the ITF waters is, however, poorly reproduced in existing ocean general circulation models (OGCMs), in which highly saline waters are transported by the ITF mainly through the Halmahera Sea (often called the "eastern route" of the ITF), resulting in significant model biases in the Indonesian Seas (Figure 1). Recent numerical studies indicated that one of the important factors causing such model biases might be vertical mixing induced by breaking of internal tides, which is not taken into account in the existing OGCMs (Jochum & Potemra, 2008; Kida & Wijffels, 2012; Koch-Larrouy et al., 2007, 2008).

Recently, Koch-Larrouy et al. (2007, 2008) modified the tidal mixing parameterization proposed by St. Laurent et al. (2002) to construct the geographical distribution of vertical diffusivities in the Indonesian Archipelago. They showed that the parameterized tidal mixing allowed the OGCM to better reproduce the ITF water mass properties within the thermocline. In their parameterization, however, two simplifying assumptions were made. First, the local dissipation efficiency $q$, the fraction of internal tide energy that dissipates near the wave generation regions, was assumed to be unity, namely, the effects of internal tide propagation were completely ignored. Second, the vertical structure function of energy dissipation $F(z)$ was artificially modified so as to confine mixing in the pycnocline. Such a vertical structure, however, obviously contradicts the realistic ones obtained from the limited direct microstructure measurements in the Indonesian Archipelago (Koch-Larrouy et al., 2015). Tidal mixing parameterizations based on such unrealistic assumptions might lead to some misunderstanding of the physical processes of the transformation of the ITF waters.

In the present study, in order to investigate the physical processes that dominate the transformation of the ITF waters, we carry out high-resolution nonhydrostatic numerical experiments in which the water mass

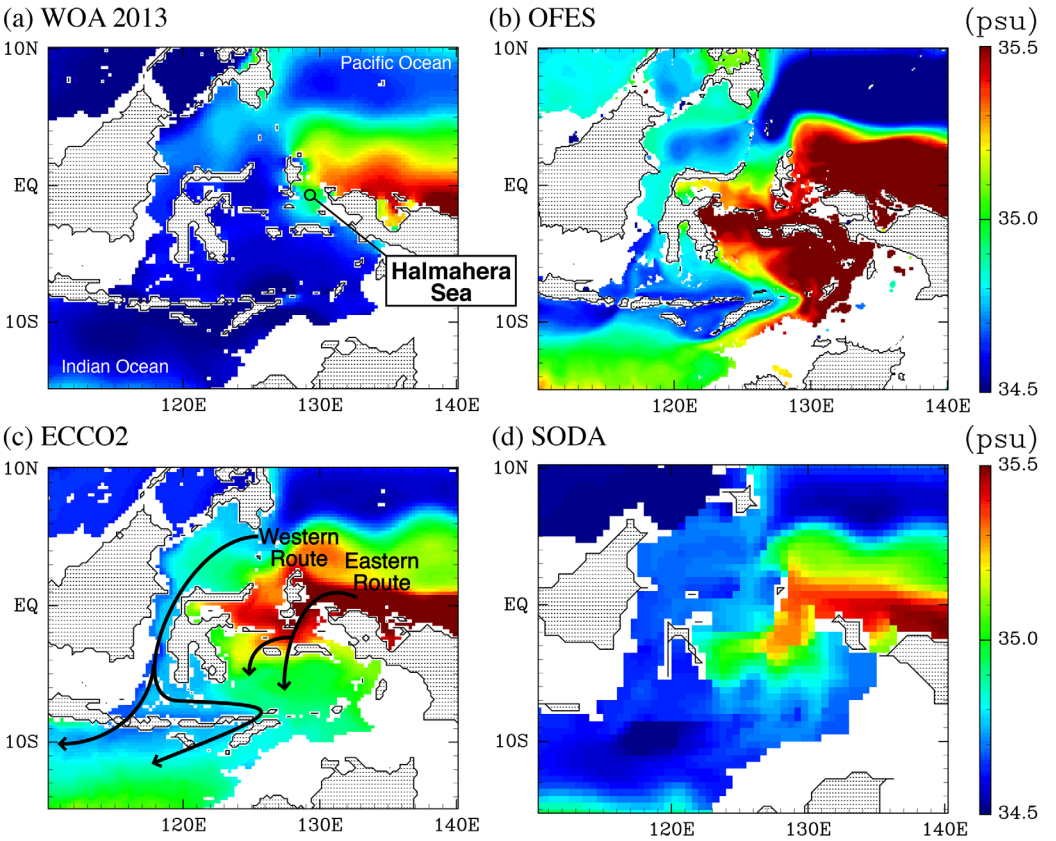


**Figure 1.** Climatological annual mean salinity at a depth of 150 m obtained from (a) World Ocean Atlas 2013, (b) OFES (OGCM for the Earth Simulator), (c) ECCO2 (Estimating the Circulation and Climate of the Ocean, Phase II), and (d) SODA (Simple Ocean Data Assimilation product). The ITF pathways are drawn schematically in Figure 1c.

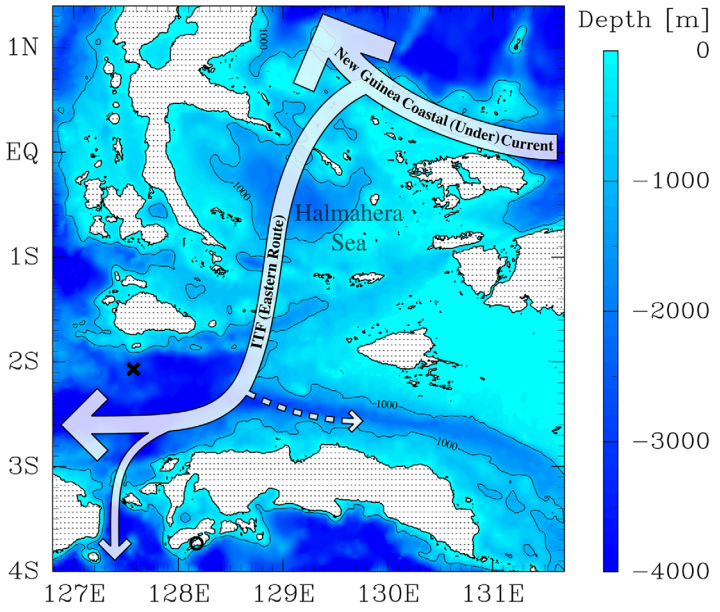


**Figure 2.** Bathymetry in the analyzed model domain. Contours indicate the 1,000 m isobath. The New Guinea Coastal (Under) Current and the ITF (eastern route) pathways are also shown schematically. Small circle and cross show the tide gauge station and TOPEX/POSEIDON crossover, respectively.

transformation is reproduced without using tidal mixing parameterization. In order to resolve the complicated topographic features in the Indonesian Archipelago, the calculation domain is limited to the Halmahera Sea where substantial transformation of the ITF waters is thought to occur.

## 2. Numerical Model

The numerical experiments are carried out using the Massachusetts Institute of Technology General Circulation Model (Marshall et al., 1997), which solves the fully nonlinear nonhydrostatic Navier-Stokes equations under the Boussinesq approximation for an incompressible fluid. The model includes the whole Halmahera Sea, covering the area from 126.8°E to 131.7°E and from 4.0°S to 1.4°N (Figure 2) with a grid spacing of $1/600^\circ$ (∼180 m) in both the longitudinal and latitudinal directions (2,940 × 3,240 grid points). The vertical grid spacing is 5 m from the ocean surface down to a depth of 300 m and gradually increased up to 700 m at the maximum depth of 4,570 m (115 vertical levels, Table 1). A spline interpolation is then applied to the high-resolution (30 arc sec) global bathymetric data set (SRTM30 PLUS, Becker et al., 2009) in order to obtain the model topography.

In the present numerical model, constant horizontal and vertical eddy viscosity coefficients $A_H = 3\ m^2\ s^{-1}$ and $A_V = 10^{-4}\ m^2\ s^{-1}$ as well as constant horizontal and vertical diffusivity coefficients $K_H = 3\ m^2\ s^{-1}$ and $K_V = 10^{-5}\ m^2\ s^{-1}$ are assumed. These are actually the smallest possible

**Table 1**
*Vertical Grid Discretization Employed in the Numerical Experiments*

| Layer numbers | $\Delta z$ (m) |
|---|---|
| 1–60 | 5.0 |
| 61–80 | 7.5 |
| 81–85 | 10.0 |
| 86–90 | 15.0 |
| 91–95 | 25.0 |
| 96–97 | 35.0 |
| 98–99 | 40.0 |
| 100–101 | 50.0 |
| 102–115 | 60.0–700.0 |

values needed to maintain the stability of the calculations (for the model sensitivity to different parameters, see Appendix A). The bottom stress is parameterized using a quadratic law with a bottom drag coefficient $C_d = 2.5 \times 10^{-3}$. At the solid boundary, a no-slip boundary condition is employed. A centered second-order advection scheme is used for momentum and tracers, so as to minimize computational diffusion caused by discretization errors of advection schemes throughout the present numerical experiments.

In order to simulate the ITF, the climatological annual mean sea surface height, temperature, and horizontal velocity fields obtained from Estimating the Circulation and Climate of the Ocean Phase II (ECCO2), which has high skill in reproducing the ITF transport (Lee et al., 2010), are used as initial and boundary conditions. Since the salty bias exists in ECCO2 within the Indonesian Seas (Figure 1), the World Ocean Atlas 2013 data set is used as initial and boundary conditions for salinity. The model is also forced along the open boundaries by applying the surface elevations of four major tidal constituents as obtained from the TPXO 7.2 global inverse tide model (Egbert & Erofeeva, 2002). The validity of the calculated surface tide fields is checked through a comparison with pelagic gage data (University of Hawaii Sea Level Center) and TOPEX/POSEIDON crossover data (taken from Robertson & Ffield, 2008) (Figure 3). To see the role of tidal forcing in the water mass transformation, the model is driven for 70 days with and without tidal forcing (hereinafter referred to as experiments Tide and NoTide, respectively). The experimental design is summarized in Table 2. Throughout this study, we focus our attention on the upper ocean (0–500 m) where the ITF is primarily confined.

## 3. Results

### 3.1. Water Mass Transformation

Salinity distributions obtained from experiments NoTide and Tide are shown in Figure 4. In experiment NoTide (Figures 4a and 4c), the ITF waters within the thermocline having a salinity maximum at depths of 100–300 m pass through the Halmahera Sea while keeping their salinity. In experiment Tide (Figures 4b and 4d), in contrast, these waters are significantly diluted before they pass through the Halmahera Sea, reducing the above mentioned model biases (Figure 5).

In order to evaluate quantitatively the water mass transformation, we next examine the dissipation of salinity variance due to background diffusivities, given by

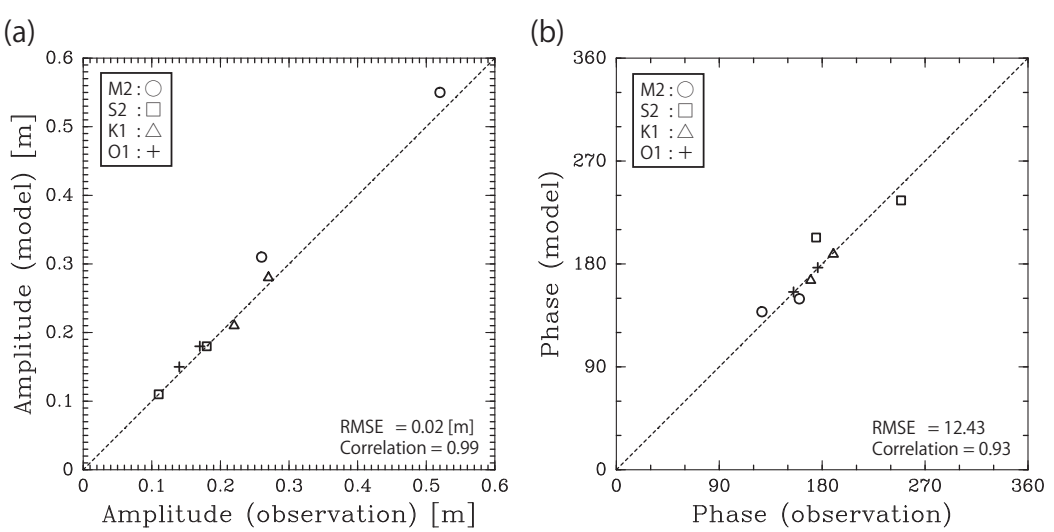


**Figure 3.** Scatterplots comparing the model-predicted tidal (a) amplitude and (b) phase with pelagic gage data and TOPEX/POSEIDON crossover data (from Robertson and Ffield, 2008, Table 1) for $M_2$ (circles), $S_2$ (squares), $K_1$ (triangles), and $O_1$ (crosses) tidal constituents.

**Table 2**
*Summary of Experimental Design*

| Experiment | NoTide | Tide | VMIX | VHMIX |
|---|---|---|---|---|
| Horizontal grid resolution | 1/600° | 1/600° | 1/120° | 1/120° |
| Background $A_H$, $K_H$ ($m^2 s^{-1}$) | 3.0 | 3.0 | 15.0 | 15.0 |
| Lateral boundary forcing | ITF | Tide and ITF | ITF | ITF |
| Parameterization of tide-induced mixing | None | None | $K_V^{Tide}$ | $K_V^{Tide}$ and $K_H^{Tide}$ |

*Note*. Values of background horizontal eddy viscosity and diffusivity used in the coarser resolution experiments (experiments VMIX and VHMIX) are increased so as to keep the grid Reynolds number ($U_0 \Delta x / A_H$) constant.

$$\chi_S = K_H \left[ \left( \frac{\partial S}{\partial x} \right)^2 + \left( \frac{\partial S}{\partial y} \right)^2 \right] + K_V \left( \frac{\partial S}{\partial z} \right)^2 \quad (1)$$

where ($x$, $y$, $z$) are Cartesian coordinates; $S$ is salinity, and $\chi_S$ is regarded as a measure of the intensity of turbulent mixing (Burchard & Rennau, 2008). Spatial patterns of $\chi_S$ (Figure 6) show that the water mass transformation is significantly enhanced in the shallow regions in the Halmahera Sea where strong tide-topography interaction is expected. In experiment Tide, the value of $\chi_S$ integrated over the Halmahera Sea (within the black rectangles shown in Figure 6) reaches $5.37 \times 10^5$ ($psu^2 m^3 s^{-1}$), which is more than twice that obtained from experiment NoTide (Table 3).

### 3.2. Internal Tides and Associated Vertical Mixing

In order to investigate the physical processes that control the water mass transformation, we next focus on internal tides and associated vertical mixing. Figure 7 shows the depth-integrated internal wave energy flux and energy dissipation rates given by

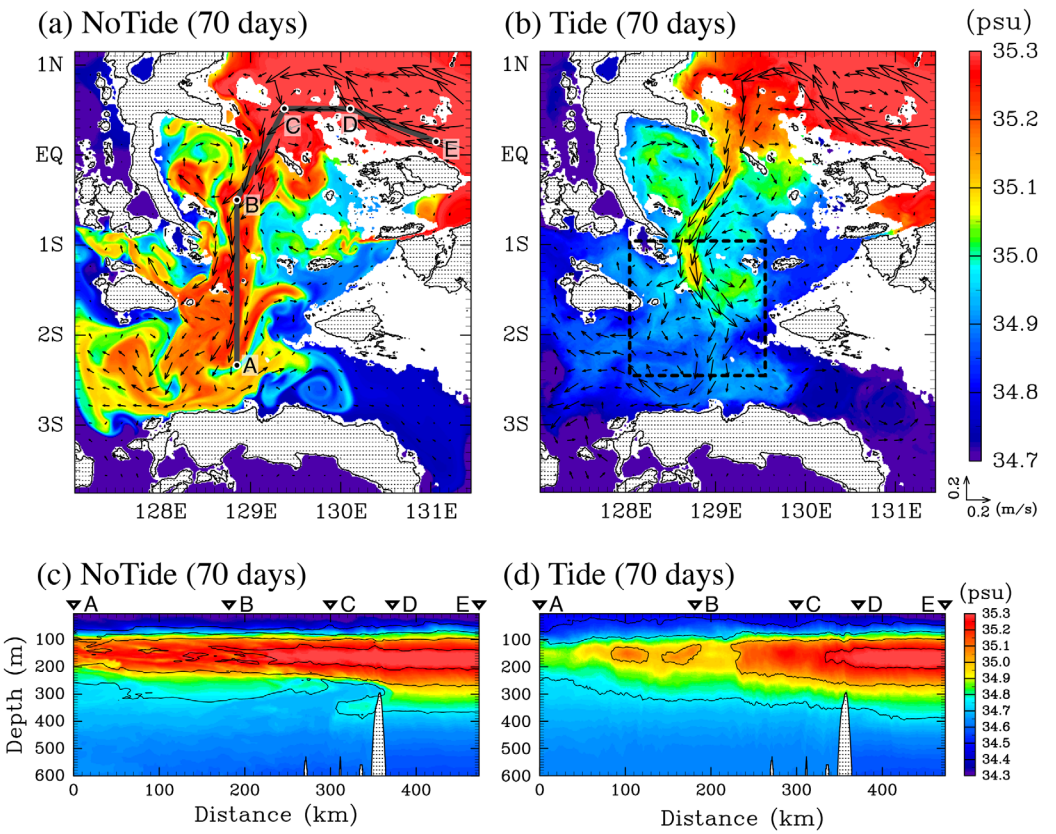


**Figure 4.** Tidally averaged salinity (color shading) and horizontal velocity (vector) after 70 days from the start of experiments (left) NoTide and (right) Tide, respectively. (a, b) Horizontal distributions at a depth of 150 m and (c, d) vertical sections along the ITF pathway (a, bold line). The dashed box in Figure 4b indicates the area for temperature-salinity plots shown in Figure 5.

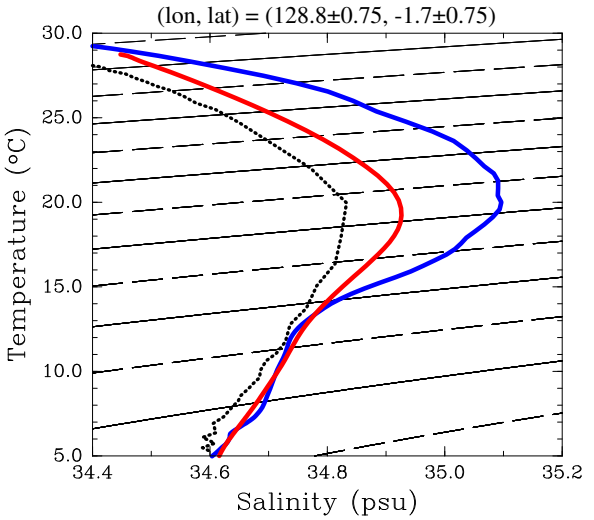


**Figure 5.** Temperature-salinity plots for the dashed box centered on 128.8°E, 1.7°S (see Figure 4b) after 70 days from the start of experiments NoTide (blue line) and Tide (red line), respectively. For comparison, the climatological annual mean values obtained from World Ocean Atlas 2013 data set are also shown (black dotted line).

$$\mathbf{F}=\overline{\mathbf{u}'_{bc}P'_{bc}}, \tag{2}$$

$$\epsilon=A_H\left[\overline{\left(\frac{\partial \mathbf{u}}{\partial x}\right)^2}+\overline{\left(\frac{\partial \mathbf{u}}{\partial y}\right)^2}\right]+A_V\overline{\left(\frac{\partial \mathbf{u}}{\partial z}\right)^2}, \tag{3}$$

respectively, where $\mathbf{u}=(u,v)$ are the velocity components in the $(x, y)$ directions; $P$ is the pressure perturbation; subscript $bc$ stands for the baroclinic component; and $\bar{}$ and $'$ denote the tidally (25 h) averaged component and the perturbation component, respectively.

It is apparent that significant energy dissipation occurs along the pathway of the ITF especially in the shallow regions from which energetic internal tides radiate away. This suggests the essential role of tide-induced vertical mixing in the transformation of the ITF waters. Unfortunately, the observational data available to check the validity of the calculated results are much limited in this area. The only available microstructure data in the Halmahera Sea were obtained during the INDOMIX cruise (Koch-Larrouy et al., 2015; P. Bouruet-Aubertot et al., personal communication, 2017). The observed vertical profiles of the energy dissipation rates are shown in Figure 8. The observed vertical distributions of energy dissipation rates generally agree well with the corresponding calculated ones, although some discrepancies can be found in the weak mixing region (S2) away from internal tide generation regions. Such discrepancies may be due to the limited capability of the present numerical model in reproducing dissipation rates smaller than the background values $\sim 3.5\times10^{-9}$ W kg$^{-1}$ estimated from Osborn's relationship $\epsilon=K_V N^2(1-R_f)/R_f$ (Osborn, 1980) with the flux Richardson number $R_f=R_iK_V/A_V$ (Stacey et al., 1999) using the critical Richardson number $R_i=0.25$, the background vertical viscosity $A_V=10^{-4}$ m$^2$s$^{-1}$ and diffusivity $K_V=10^{-5}$ m$^2$s$^{-1}$, and the buoyancy frequency averaged over a depth range of 200–1,500 m $N\sim 3\times10^{-3}$ s$^{-1}$, respectively.

## 4. Discussion

In order to identify the physical processes responsible for the transformation of the ITF waters, we isolate here the effect of tide-induced vertical mixing through following procedures:

1. Excluding the existence of the ITF by assuming horizontally uniform background density stratification, we first carry out a numerical experiment forced only by tides. The model configuration is the same as

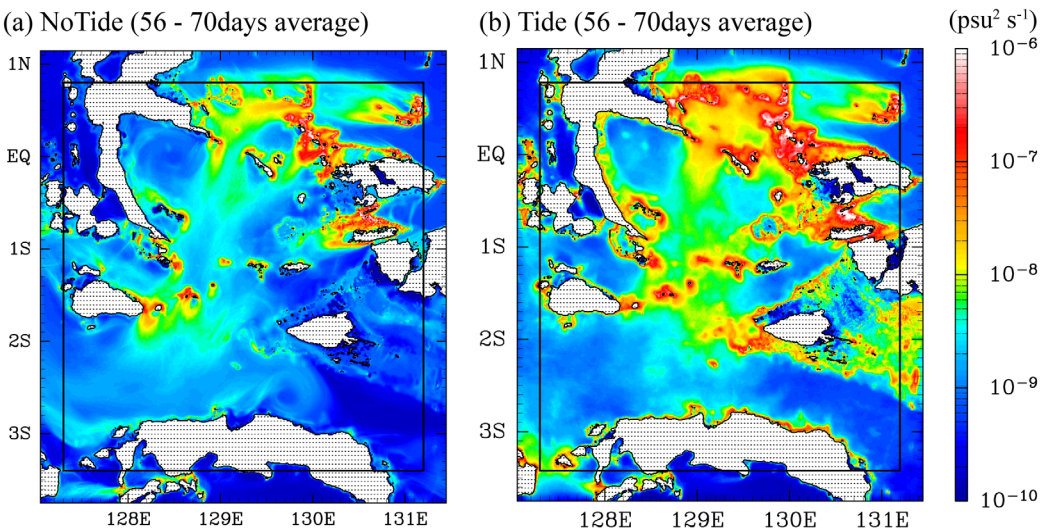


**Figure 6.** Spatial distributions of $\chi_S$ averaged over the spring-neap tidal cycle and over a depth range of 0−500 m ((a) NoTide; (b) Tide).

**Table 3**
*Value of $\chi_S$ Integrated Over the Whole Analyzed Model Domain for Each Experiment*

| Experiment | NoTide | Tide | VMIX | VHMIX |
|---|---|---|---|---|
| $\int \chi_S dV \times 10^5 (\mathrm{psu^2 m^3 s^{-1}})$ | 2.14 | 5.37 | 4.47 | 4.90 |
| Contribution | – | – | 76% | 90% |

*Note.* Each contribution to the tide-induced water mass transformation is defined as $(\int \chi_s^{\mathrm{VMIX\ or\ VHMIX}} dV - \int \chi_s^{\mathrm{A1}} dV)/(\int \chi_s^{\mathrm{Tide}} dV - \int \chi_s^{\mathrm{NoTide}} dV)$, where $\int \chi_S^{\mathrm{ExperimentName}} dV$ represents the value of $\chi_S$ integrated over the whole analyzed model domain for each experiment. The model configuration of experiment A1 is the same as experiment NoTide but for the decreased horizontal grid resolution (1/120°). For details about experiment A1, see Appendix A and Table A1.

experiment Tide but for the background density stratification obtained by horizontally averaging the initial density stratification employed in section 3.

2. Using the calculated energy dissipation rates ($\epsilon$) and local buoyancy frequency ($N$), the vertical diffusivity is estimated following Osborn's relationship such that

$$K_V^{\mathrm{Tide}} = \Gamma \frac{\epsilon}{N^2} \tag{4}$$

where $\Gamma$ is the mixing efficiency assumed to be 0.2. The vertically averaged distribution of the vertical diffusivity is shown in Figure 9a.

The distribution of the parameterized vertical eddy diffusivity (Figure 9a) shows that mixing hotspots with $K_V^{\mathrm{Tide}} \sim 10^{-2}\,\mathrm{m^2 s^{-1}}$ are found in the shallow regions in the Halmahera Sea. To investigate the effect of tide-induced vertical mixing on the transformation of the ITF waters, we next carry out an additional numerical experiment which takes into account the distribution of $K_V^{\mathrm{Tide}}$ instead of applying tidal forcing at the open boundaries (hereinafter referred to as experiment VMIX). Note that the horizontal grid resolution of experiment VMIX is decreased to $1/120^\circ$ (see Table 2 for details). Despite the coarser horizontal grid resolution, the predicted water mass transformation is hardly affected (for details, see Appendix A). Figure 10a shows the calculated salinity distribution at a depth of 150 m. In the south of Halmahera Sea, salinity obtained from experiment VMIX is slightly higher than that obtained from experiment Tide (Figure 4a), but is much reduced than that obtained from experiment NoTide (Figure 4b). The value of $\chi_S$ integrated over the Halmahera Sea shows that the effect of tide-induced vertical mixing can account for 76% of the tide-induced water mass transformation (Table 3). This implies that the transformation of the ITF waters is dominated by tide-induced vertical mixing, although there must be some additional mechanisms to make up for the lack of water mass transformation as is discussed in Appendix B.

## 5. Concluding Remarks

In the present study, to clarify the physical mechanisms that control the transformation of the ITF waters in the Halmahera Sea which is thought to be the most important bottleneck in simulating the transformation of the ITF waters, we have carried out high-resolution ($\Delta x, \Delta y \sim 180\,\mathrm{m}$) nonhydrostatic three-dimensional

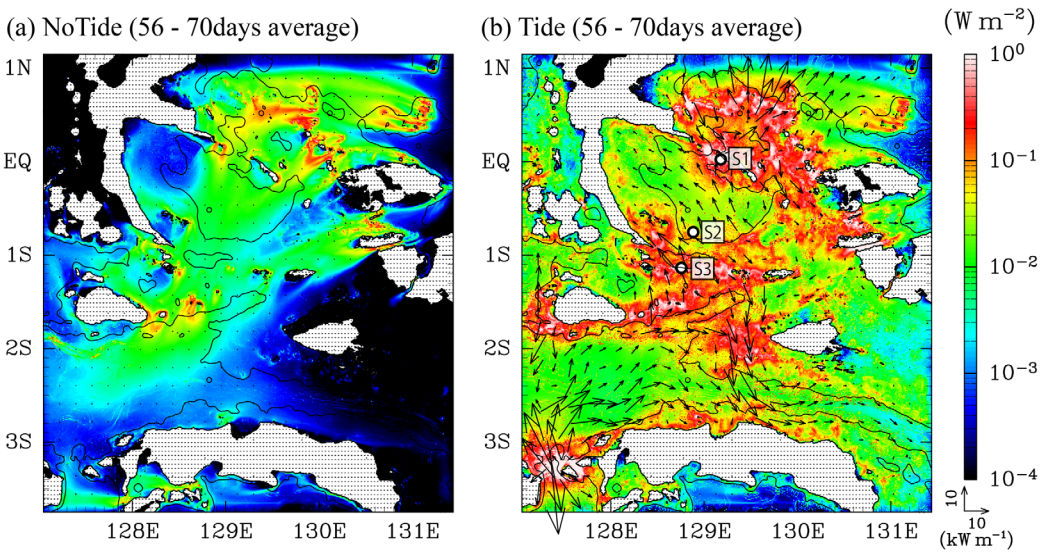


**Figure 7.** Spatial distributions of depth-integrated internal wave energy flux (vector) and energy dissipation rates (color shading) averaged over the spring-neap tidal cycle ((a) NoTide; (b) Tide). Contours indicate the 1,000 m isobath.

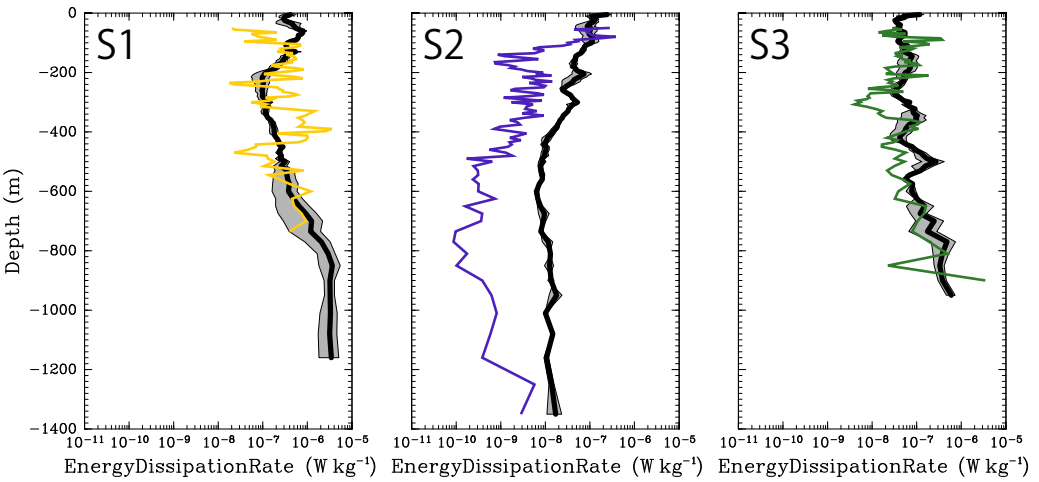


**Figure 8.** Comparison of the vertical profiles of the energy dissipation rates obtained from experiment Tide (black lines) and direct microstructure measurements (colored lines) at S1, S2, and S3 (shown in Figure 7b), respectively. Thick and thin black lines show the values averaged over the spring-neap tidal cycle and the values at spring or neap tide, respectively. For details about the processing of microstructure data, readers are referred to Koch-Larrouy et al. (2015).

numerical experiments with and without realistic tidal forcing. It has been shown that, in the experiment with (or without) tidal forcing, the ITF waters are significantly (or hardly) diluted while passing through the shallow regions in the Halmahera Sea, where intensive vertical mixing is induced by breaking of internal tides resulting from strong tide-topography interaction. As a result, large model biases are much reduced by taking into account the existence of tides. To identify the physical processes responsible for the transformation of the ITF waters, we have isolated the effect of tide-induced vertical mixing using Osborn's relationship and incorporated it into the numerical model instead of applying tidal forcing at the open boundaries. It has been shown that tide-induced vertical mixing can account for 76% of the tide-induced transformation of the ITF waters.

One of the candidates that can account for the remaining water mass transformation is tide-induced "horizontal mixing." Actually, supplementary contribution of horizontal mixing to the water mass transformation is demonstrated by an additional numerical experiment (for details, see Appendix B) where parameterized

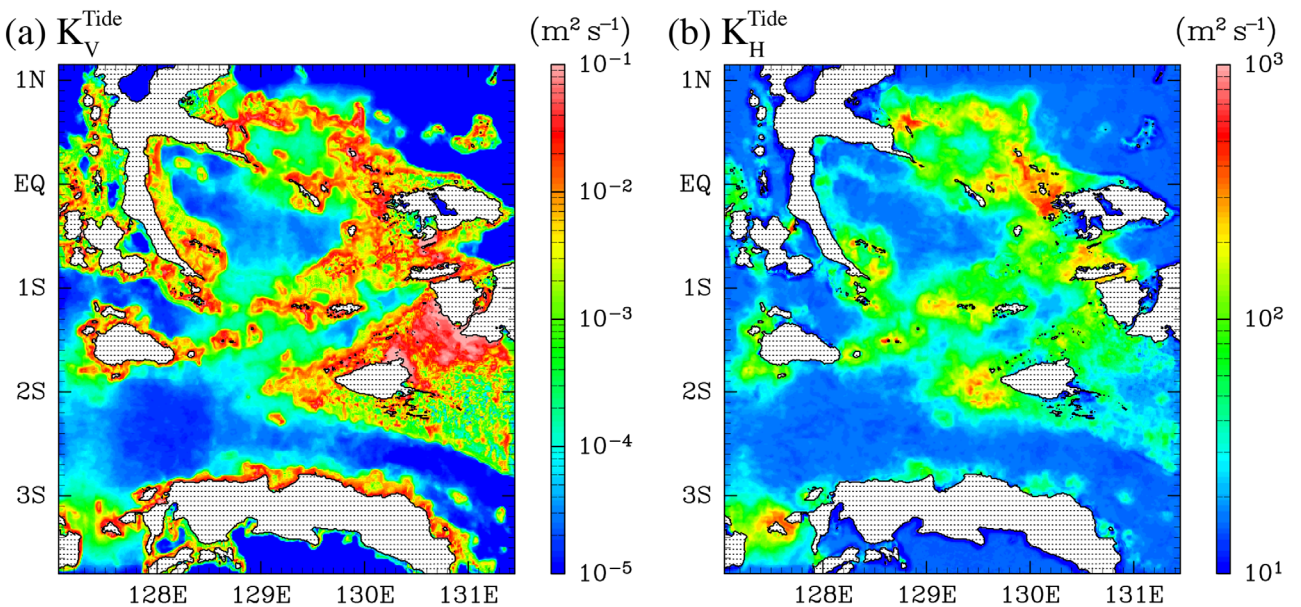


**Figure 9.** Model-predicted distributions of (a) vertical and (b) horizontal eddy diffusivities both averaged over the spring-neap tidal cycle and over a depth range of 0−500 m, respectively.

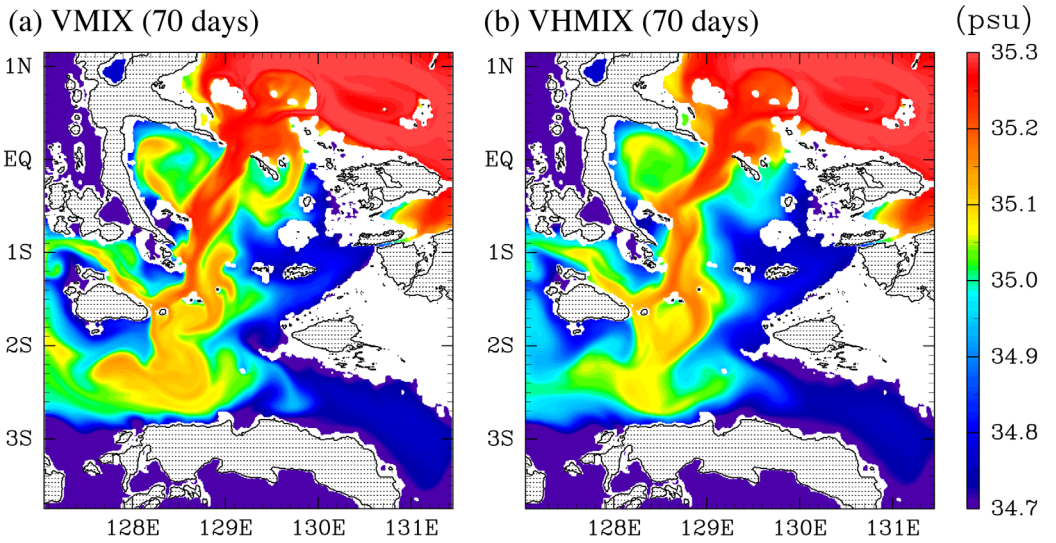


**Figure 10.** As in Figures 4a and 4b but for experiments (a) VMIX and (b) VHMIX, respectively.

effect of horizontal mixing is associated with the submesoscale eddies resulting from tidal interaction with land configurations.

Needless to say, there must be some ambiguity in the water mass transformation calculated in the present numerical experiments. First, it might not be allowed to assess separately the contributions of tidal flow and the ITF to the mixing processes in the Halmahera Sea which are actually linked with the magnitude of the combined flow. Second, it remains unclear whether or not the grid resolution employed in the present numerical experiments is fine enough to reproduce the transformation of the ITF waters. Although the observed vertical distributions of energy dissipation rates generally agree well with the corresponding calculated ones, some discrepancies are recognized in the weak mixing region away from internal tide generation regions. This motivates us to assess the validity of the present model results (e.g., $\epsilon$ and $\chi_S$) through more extensive microstructure observations in the Halmahera Sea together with simultaneous surveys of internal wavefields, the results of which will be reported elsewhere.

## Appendix A: Sensitivity of the Water Mass Transformation to Various Parameters

Here we concentrate on the sensitivity of the calculated results to (1) the horizontal and vertical grid spacing, and (2) the background viscosity and diffusivity. For each experiment, we calculate the value of $\chi_S$ integrated over the whole analyzed model domain. The summary of the sensitivity experiments is listed in Table A1.

The sensitivity to the horizontal and/or vertical grid spacing is examined through each of experiments A1, A2, and A3, where the model configuration is the same as in experiment NoTide or Tide, but for the grid

**Table A1**
*Summary of Sensitivity Experiments*

| | A1 | A2 | A3 | B1 | B2 |
|---|---|---|---|---|---|
| Horizontal grid resolution | 1/120° | 1/120° | 1/120° | 1/600° | 1/600° |
| Vertical grid resolution (m) | 5.0∼ | 5.0∼ | 25.0∼ | 5.0∼ | 5.0∼ |
| Background $A_H$, $K_H$ ($m^2s^{-1}$) | 15.0 | 15.0 | 15.0 | 15.0 | 0.2 |
| Background $A_V \times 10^{-4}$ ($m^2s^{-1}$) | 1.0 | 1.0 | 5.0 | 5.0 | 0.2 |
| Background $K_V \times 10^{-5}$ ($m^2s^{-1}$) | 1.0 | 1.0 | 5.0 | 5.0 | 0.2 |
| Lateral boundary forcing | ITF | Tide and ITF | Tide and ITF | Tide and ITF | Tide and ITF |
| $\int \chi_S dV \times 10^5$ ($psu^2m^3s^{-1}$) | 2.01 | 5.53 | 5.05 | 5.20 | – |

*Note*. Values of background horizontal/vertical eddy viscosity and diffusivity used in the coarser resolution experiments (A1, A2 and A3) are increased so as to keep the grid Reynolds number ($U_0\Delta x/A_H$ or $U_0\Delta z/A_V$) constant. In experiment A3, the vertical grid resolution is decreased to 25 m at all the depths shallower than 700 m.

spacing (see Table A1 for details). We can see that even when the horizontal (or both horizontal and vertical) grid spacing is increased by a factor of 5, the integrated value of $\chi_S$ is hardly affected.

The sensitivity to the background viscosity and diffusivity, on the other hand, is examined through each of experiments B1 and B2. In experiment B1, although all the viscosity and diffusivity coefficients are increased by a factor of 5, the integrated value of $\chi_S$ does not change appreciably. It is interesting to note that the vertical profiles of the energy dissipation rates obtained from experiment B1 agree well with the corresponding observed ones

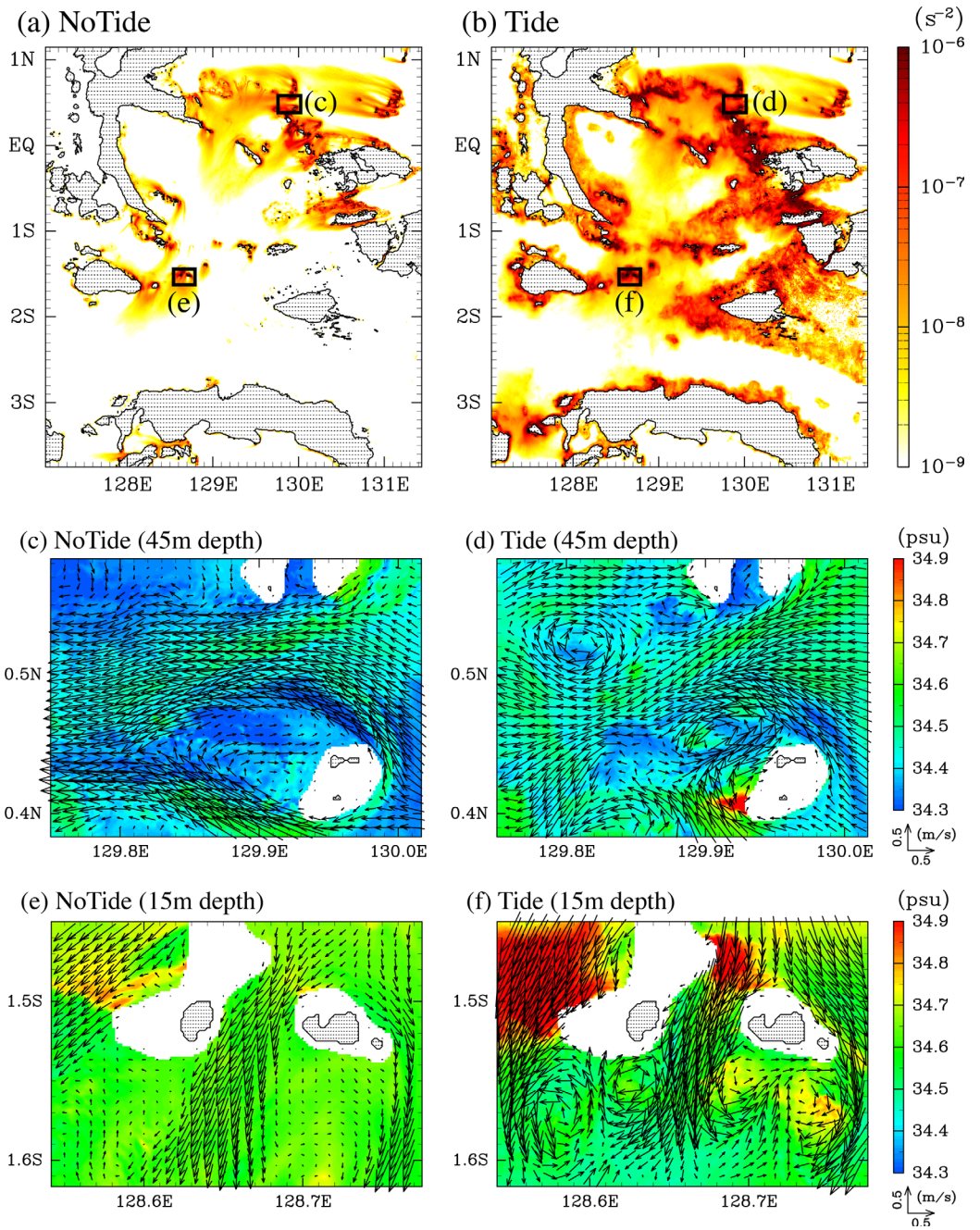


**Figure B1.** (a, b) Spatial distributions of enstrophy obtained from experiments (left) NoTide and (right) Tide, both averaged over the spring-neap tidal cycle and over a depth range of 0−500 m. (c–f) Snap shots of salinity (color shading) and horizontal current velocity (vector) obtained from experiments NoTide and Tide for the areas shown by black rectangles in Figures A1a and A1b, respectively. Submesoscale eddies with a diameter of a few kilometers are generated by tidal interaction with complicated land configurations.

especially at the mixing hotspots such as S1 and S3 (figures not shown). This is because the current shears are decreased so as to compensate the increased viscosity coefficients. In contrast, when all the viscosity and diffusivity coefficients are decreased by a factor of 5 (experiment B2), the calculation becomes computationally unstable.

## Appendix B: Effect of Tide-Induced Horizontal Mixing on the Transformation of the ITF Waters

As mentioned in the previous studies (Gordon, 2005; Koch-Larrouy et al., 2008), horizontal mixing is another candidate responsible for the transformation of the ITF waters. Actually, the distributions of horizontal velocity and enstrophy obtained from experiment Tide show that a number of submesoscale eddies are induced in the archipelagos by tidal flow interaction with complicated land configurations (Figure B1). We next investigate quantitatively the roles of horizontal mixing induced by these submesoscale eddies in transforming the ITF waters. We isolate here the effect of tide-induced horizontal mixing by taking the following procedures:

1. We first carry out a numerical experiment forced only by tides (the same experiment as in section 4).
2. We next track a number of labeled particles, each initially placed at the center of the grid and passively advected by the calculated three-dimensional tidal velocity field. The effects of the background diffusion coefficient assumed in the present numerical experiments ($K_H = 3\,m^2\,s^{-1}$, $K_V = 10^{-5}\,m^2\,s^{-1}$) are equivalently expressed in terms of random displacement of particles, called "random walk" (Cushman-Roisin & Beckers, 2011).
3. As a measure of the spreading of particles, we define tide-induced horizontal eddy diffusivity (Hatayama et al., 1996),

$$K_H^{\mathrm{Tide}}(\mathbf{X}_{IJK}, t) = \frac{1}{2}\frac{\sigma_H^2(\mathbf{X}_{IJK}, t) - \sigma_H^2(\mathbf{X}_{IJK}, t-\Delta T)}{\Delta T}. \tag{B1}$$

with

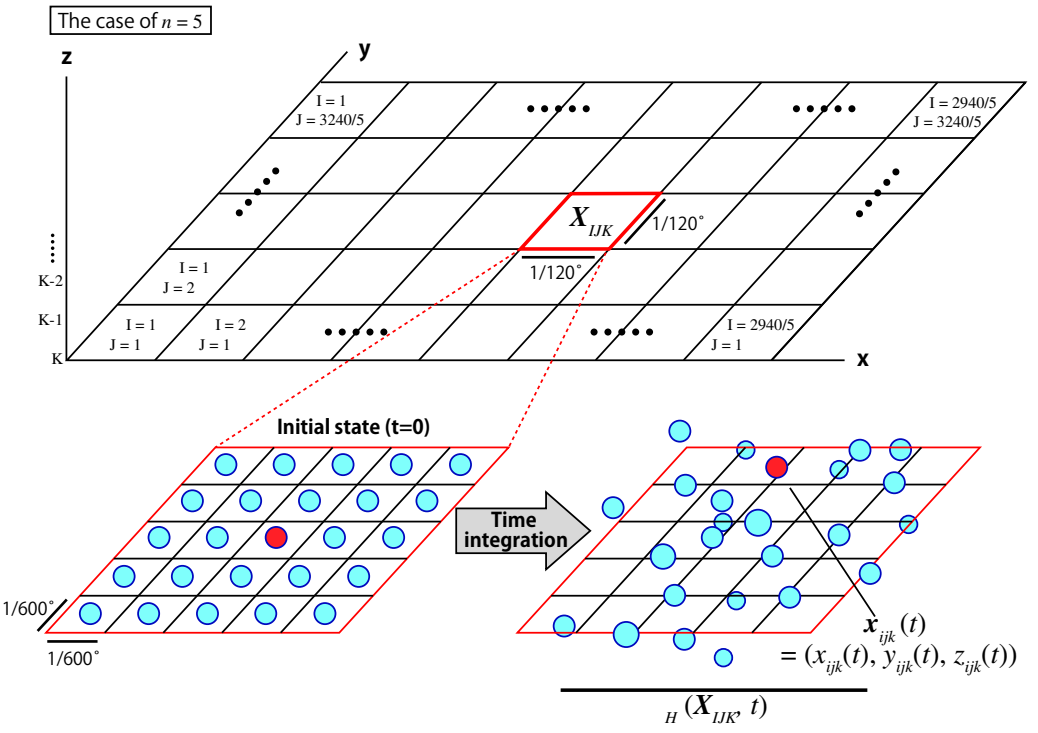


**Figure B2.** Schematic of the Lagrangian particle tracking method for the case of $n = 5$.

$$\sigma_{\mathrm{H}}^2(\mathbf{X}_{IJK},t)=\frac{1}{2n^2}\sum_{i'=1}^{n}\sum_{j'=1}^{n}\left(\left(x_{ijk}(t)-\langle x_{IJK}(t)\rangle\right)^2+\left(y_{ijk}(t)-\langle y_{IJK}(t)\rangle\right)^2\right) \quad (B2)$$

$$(i=n(I-1)+i',j=n(J-1)+j',k=K),$$

where $\Delta T$ is the time interval (25 h); $\mathbf{X}_{IJK}=(X_{IJK},Y_{IJK},Z_{IJK})$ denotes the position of each area at which horizontal eddy diffusivity is calculated ($I=1,\ldots 2,940/n$; $J=1,\ldots 3,240/n$; $K=1,\ldots 115$); $\mathbf{x}_{ijk}=(x_{ijk}(t),y_{ijk}(t),z_{ijk}(t))$ denotes the position of each particle in Cartesian coordinates at time $t$ ($i=1,\ldots 2,940$; $j=1,\ldots 3,240$; $k=1,\ldots 115$); $\sigma^2$ indicates the variance of vertical particle displacements relative to the center of mass $\langle x_{IJK}\rangle$ $(=\sum_{i'=1}^{n}\sum_{j'=1}^{n}x_{ijk}/n^2)$ at time $t$ (Figure B2). Note that we assume here $n=5$, so that $K_{\mathrm{H}}^{\mathrm{Tide}}$ parameterizes subgrid-scale processes for each $1/120^\circ\times 1/120^\circ$ square.

Note that equation (5) is appropriate only when $\sigma_{\mathrm{H}}^2$ is proportional to $t$, namely, only when $K_{\mathrm{H}}^{\mathrm{Tide}}$ is constant. The area-averaged value of $K_{\mathrm{H}}^{\mathrm{Tide}}(t)$ in each layer actually settles into an approximately steady state after the $M_2$ tidal period (12.41 h) (figures not shown).

The distribution of $K_{\mathrm{H}}^{\mathrm{Tide}}$ in the archipelagos (Figure 9b) shows that horizontal mixing becomes significant at the locations where tide-induced eddies are created. Figure 10b shows the distribution of salinity in the thermocline obtained by incorporating both $K_{\mathrm{V}}^{\mathrm{Tide}}$ and $K_{\mathrm{H}}^{\mathrm{Tide}}$ into the numerical model instead of applying tidal forcing at the open boundaries (hereinafter referred to as experiment VHMIX, see Table 2 for details). It can be seen that salinity in the south of the Halmahera Sea is slightly reduced compared with the corresponding value obtained from experiment VMIX. The value of $\chi_S$ integrated over the Halmahera Sea shows that the combined effect of tide-induced vertical and horizontal mixing can account for 90% of the tide-induced water mass transformation (Table 3), indicating the nonnegligible role of tide-induced horizontal mixing in the water mass transformation.

**Acknowledgments**

The bathymetric data were obtained from SRTM30PLUS (http://topex.ucsd.edu/www_html/srtm30_plus.html), the sea surface height, temperature, and velocity data from Estimating the Circulation and Climate of the Ocean Phase II (ECCO2, http://ecco2.jpl.nasa.gov), the salinity data from the World Ocean Atlas 2013 (https://www.nodc.noaa.gov/OC5/woa13/woa13data.html), OGCM for the Earth Simulator (OFES, http://www.jamstec.go.jp/esc/research/AtmOcn/product/ofes.html), and Simple Ocean Data Assimilation product (SODA, http://www.atmos.umd.edu/~ocean/data.html or soda.tamu.edu), the tide gauge data from the University of Hawaii Sea Level Center (http://uhslc.soest.hawaii.edu), the barotropic tidal current velocity and surface elevation used for the boundary condition from the TPXO 7.2 global inverse tide model (http://volkov.oce.orst.edu/tides/global.html), and the TOPEX/POSEIDON crossover data were taken from Robertson and Ffield (2008). Model results are publicly available at http://www-aos.eps.s.u-tokyo.ac.jp/~nagai_t/NH2017Data/. Figures were produced using the GFD-DENNOU Library. This work was supported by the Japan Society for the Promotion of Science (JSPS) KAKENHI grants 26257208 and 15H05824.

## References

Becker, J. J., Sandwell, D. T., Smith, W. H. F., Braud, J., Binder, B., Depner, J., . . . Weatherall, P. (2009). Global bathymetry and elevation data at 30 arc seconds resolution: SRTM30 PLUS. *Marine Geodesy*, *32*, 355–371. https://doi.org/10.1080/01490410903297766

Burchard, H., & Rennau, H. (2008). Comparative quantification of physically and numerically induced mixing in ocean models. *Ocean Modelling*, *20*, 293–311. https://doi.org/10.1016/j.ocemod.2007.10.003

Cushman-Roisin, B., & Beckers, J. M. (2011). *Introduction to geophysical fluid dynamics: Physical and numerical aspects*. Cambridge, MA: Academic Press.

Egbert, G. D., & Erofeeva, S. Y. (2002). Efficient inverse modeling of barotropic ocean tides. *Journal of Atmospheric and Oceanic Technology*, *19*(2), 183–204.

Gordon, A. L. (2005). Oceanography of the Indonesian Seas and their throughflow. *Oceanography*, *18*, 14–27.

Hatayama, T., Awaji, T., & Akitomo, K. (1996). Tidal currents in the Indonesian Seas and their effect on transport and mixing. *Journal of Geophysical Research*, *101*(C5), 12353–12373.

Jochum, M., & Potemra, J. (2008). Sensitivity of tropical rainfall to Banda Sea diffusivity in the community climate system model. *Journal of Climate*, *21*, 6445–6454. https://doi.org/10.1175/2008JCLI2230.1

Kida, S., & Wijffels, S. (2012). The impact of the Indonesian Throughflow and tidal mixing on the summertime sea surface temperature in the western Indonesian Seas. *Journal of Geophysical Research: Oceans*, *117*, C09007. https://doi.org/10.1029/2012JC008162

Koch-Larrouy, A., Atmadipoera, A., van Beek, P., Madec, G., Aucan, J., Lyard, F., . . . Souhaut, M. (2015). Estimates of tidal mixing in the Indonesian archipelago from multidisciplinary INDOMIX *in-situ* data. *Deep-Sea Research Part I: Oceanographic Research Papers*, *106*, 136–153.

Koch-Larrouy, A., Madec, G., Bouruet-Aubertot, P., Gerkema, T., Bessieres, L., & Molcard, R. (2007). On the transformation of Pacific Water into Indonesian Throughflow Water by internal tidal mixing. *Geophysical Research Letters*, *34*, L04604. https://doi.org/10.1029/2006GL028405

Koch-Larrouy, A., Madec, G., Iudicone, D., Atmadipoera, A., & Molcard, R. (2008). Physical processes contributing to the water mass transformation of the Indonesian Throughflow. *Ocean Dynamics*, *58*, 275–288. https://doi.org/10.1007/s10236-008-0154-5

Lee, T., Awaji, T., Balmaseda, M., Ferry, N., Fujii, Y., Fukumori, I., . . . Weaver, A. (2010). Consistency and fidelity of Indonesian-throughflow total volume transport estimated by 14 ocean data assimilation products. *Dynamics of Atmospheres and Oceans*, *50*, 201–223. https://doi.org/10.1016/j.dynatmoce.2009.12.004

Marshall, J., Adcroft, A., Hill, C., Perelman, L., & Heisey, C. (1997). A finite-volume, incompressible Navier Stokes model for studies of the ocean on parallel computers. *Journal of Geophysical Research*, *102*(C3), 5753–5766.

Osborn, T. R. (1980). Estimates of the local rate of vertical diffusion from dissipation measurements. *Journal of Physical Oceanography*, *10*, 83–89.

Robertson, R., & Ffield, A. (2008). Baroclinic tides in the Indonesian Seas: Tidal fields and comparisons to observations. *Journal of Geophysical Research*, *113*, C07031. https://doi.org/10.1029/2007JC004677

Stacey, M. T., Monismith, S. G., & Burau, J. R. (1999). Observations of turbulence in a partially stratified estuary. *Journal of Physical Oceanography*, *29*, 1950–1970.

St. Laurent, L. C., Simmons, H. L., & Jayne, S. R. (2002). Estimating tidally driven mixing in the deep ocean. *Geophysical Research Letters*, *29*(23), 2106. https://doi.org/10.1029/2002GL015633

Tomczak, M., & Godfrey, J. S. (2003). *Regional oceanography: An introduction* (391 pp.). Oxford, UK: Elsevier.